

Growth and Characterization of Metalorganic Vapor-Phase Epitaxy-Grown β -(Al_xGa_{1-x})₂O₃/β-Ga₂O₃ Heterostructure Channels

Praneeth Ranga^{1, a)}, Arkka Bhattacharyya^{1, a)}, Adrian Chmielewski², Saurav Roy¹, Rujun Sun¹, Michael A. Scarpulla^{1,3}, Nasim Alem² and Sriram Krishnamoorthy¹

¹*Department of Electrical and Computer Engineering, The University of Utah, Salt Lake City, UT 84112, USA*

²*Department of Materials Science and Engineering, Pennsylvania State University, University Park, PA 16802, USA*

³*Department of Materials Science and Engineering, University of Utah, Salt Lake City, Utah 84112, USA*

^{a)} *Praneeth Ranga and Arkka Bhattacharyya contributed equally*

E-mail: praneeth.ranga@utah.edu, sriram.krishnamoorthy@utah.edu

We report on the growth and characterization of metalorganic vapor-phase epitaxy-grown β -(Al_xGa_{1-x})₂O₃/β-Ga₂O₃ modulation-doped heterostructures. Electron channel is realized in the heterostructure by utilizing a delta-doped β -(Al_xGa_{1-x})₂O₃ barrier. Electron channel characteristics are studied using transfer length method, capacitance-voltage and Hall measurements. Hall sheet charge density of $1.06 \times 10^{13} \text{ cm}^{-2}$ and mobility of $111 \text{ cm}^2/\text{Vs}$ is measured at room temperature. Fabricated transistor showed peak current of 22 mA/mm and on-off ratio of 8×10^6 . Sheet resistance of 5.3 kΩ/Square is measured at room temperature, which includes contribution from a parallel channel in β -(Al_xGa_{1-x})₂O₃.

Ultrawide bandgap materials such as β -Ga₂O₃ has attracted a lot of interest because of their suitable properties for high-power electronics and deep-UV optoelectronic applications. The high bandgap (~4.6 eV) results in a very large predicted breakdown field strength of 6-8 MV/cm, which is much larger than other wide bandgap materials like GaN and SiC¹). Significant advances have been made in growth²⁻⁵), characterization, and fabrication of β -Ga₂O₃ devices within the last decade⁶). Vertical and lateral devices with high breakdown voltages and high critical fields have been demonstrated by multiple research groups⁷⁻¹¹).

Room temperature mobility of uniformly-doped β -Ga₂O₃ is limited by polar optical phonon scattering, which limits the maximum mobility to ~200 cm²/Vs¹²). In modulation-doped 2DEG channel, mobility is not limited by impurity scattering unlike doped semiconductors. This is due to the absence of ionized impurity donors in the electron channel. For realizing a 2DEG, growth of high-quality modulation-doped β -(Al_xGa_{1-x})₂O₃/ β -Ga₂O₃ heterostructure with sharp dopant profile is necessary. Theoretical studies indicate that β -(Al_xGa_{1-x})₂O₃ is stable up to a composition of ~x = 0.8 which has a bandgap of ~6.5 eV¹³). Moreover, DFT calculations indicate that n-type shallow doping is achievable for the entire composition range of stable β -(Al_xGa_{1-x})₂O₃¹⁴). All the above material properties suggest that formation of 2DEG at β -(Al_xGa_{1-x})₂O₃/ β -Ga₂O₃ is very favorable. Recently reported transport calculations performed by Kumar et.al indicate that mobility of a 2DEG can significantly exceed that of bulk β -Ga₂O₃¹⁵). This is expected to happen when the 2DEG sheet charge exceeds 5 x 10¹² cm⁻². At high charge densities (n_s > 5 x 10¹² cm⁻²), the plasmon screening of LO (longitudinal optical) phonons leads to increase in polar optical phonon (POP) limited mobility¹⁵). Having a high 2DEG sheet charge and mobility can lead to a significant improvement in device performance over conventional β -Ga₂O₃ devices.

Demonstration of β -(Al_xGa_{1-x})₂O₃/ β -Ga₂O₃ heterostructure modulation-doped field effect transistors (MODFET) has already been made using MBE-grown material^{16,17}). All the current literature is based on MBE-grown β -(Al_xGa_{1-x})₂O₃/ β -Ga₂O₃ heterostructures¹⁶⁻²¹). 2DEG sheet charge densities between 1x10¹² - 5 x10¹² cm⁻² and mobilities of 75 -180 cm²/Vs

have been achieved using MBE technique^{16,18–21}). Currently the maximum sheet charge density reported in MBE-grown $\beta\text{-(Al}_x\text{Ga}_{1-x}\text{)}_2\text{O}_3/\beta\text{-Ga}_2\text{O}_3$ is less than $5 \times 10^{12} \text{ cm}^{-2}$ for a single heterostructure without parallel channel in $\beta\text{-(Al}_x\text{Ga}_{1-x}\text{)}_2\text{O}_3$ ²⁰). Recently, MOVPE (metalorganic vapor-phase epitaxy) has emerged as a promising technique for high-quality $\beta\text{-Ga}_2\text{O}_3$. Uniformly-doped $\beta\text{-Ga}_2\text{O}_3$ films with high room temperature mobility values have been demonstrated^{3,22–24}). High composition MOVPE-grown (100)-oriented $\beta\text{-(Al}_x\text{Ga}_{1-x}\text{)}_2\text{O}_3$ films with $x \sim 0.52$ has been realized recently²⁵). N-type doping of MOVPE-grown $\beta\text{-(Al}_x\text{Ga}_{1-x}\text{)}_2\text{O}_3$ films with composition up to $x \sim 0.3$ has already been demonstrated^{26,27}). In addition, delta-doped $\beta\text{-Ga}_2\text{O}_3$ films with sheet charge up to $1 \times 10^{13} \text{ cm}^{-2}$ is reported using MOVPE²⁸). For achieving sharp dopant profiles with low FWHM (full width at half maximum), it is necessary to suppress surface segregation of donor atoms. Our recent work on MOVPE-grown delta-doped films grown at low temperatures suggests that by suppressing surface segregation of Si delta sheets with FWHM comparable to MBE-grown films can be realized²⁹). All the above factors indicate the promise of MOVPE technique for studying high charge density $\beta\text{-(Al}_x\text{Ga}_{1-x}\text{)}_2\text{O}_3/\beta\text{-Ga}_2\text{O}_3$ heterostructures.

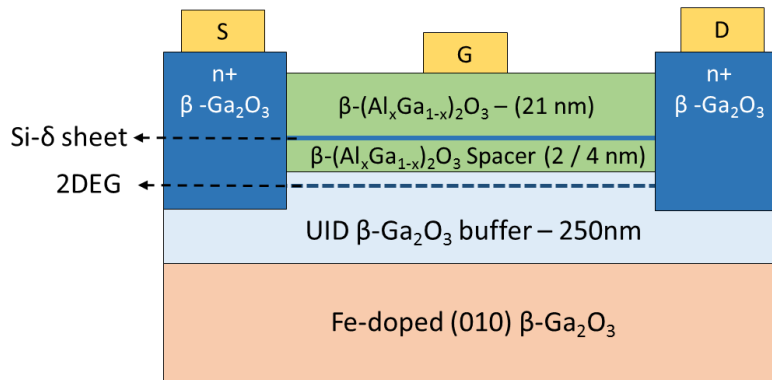


Fig.1 Schematic of MOVPE-grown $\beta\text{-(Al}_x\text{Ga}_{1-x}\text{)}_2\text{O}_3/\beta\text{-Ga}_2\text{O}_3$ heterostructure FET (HFET) with regrown ohmic contacts. (Sample A spacer layer thickness- 4 nm; Sample B spacer layer thickness- 2 nm).

$\beta\text{-(Al}_x\text{Ga}_{1-x}\text{)}_2\text{O}_3/\beta\text{-Ga}_2\text{O}_3$ heterostructures are grown using Agnitron Agilis using TEGa (Triethyl Gallium), TMAI (Trimethyl Aluminium) and O_2 (oxygen) as precursors and Argon as carrier gas. The following growth parameters are utilized – Alkyl flow – $5.26 \mu\text{mol/min}$,

O_2 – 500 sccm, Pressure - 15 Torr, Temperature - 650 °C. Growth is performed on Fe-doped (010) β - Ga_2O_3 substrates from Novel Crystal Technology. As-received substrates are cleaned with Acetone, Methanol and DI water followed a HF dip for 20 mins. A schematic of the grown β - $(Al_xGa_{1-x})_2O_3/\beta$ - Ga_2O_3 heterostructure is shown in fig.1. The film consists of a 250 nm UID β - Ga_2O_3 buffer layer followed by a thin β - $(Al_xGa_{1-x})_2O_3$ spacer layer (2 / 4 nm) and a thick β - $(Al_xGa_{1-x})_2O_3$ barrier (21 nm). Next, delta doping of β - $(Al_xGa_{1-x})_2O_3$ layer is performed by using a growth interruption process. The process consists of a growth interruption step with a pre- and post-purge steps (30 secs) before and after the delta doping. The delta sheet density is controlled by changing the silane flow period (60 secs) and the silane gas flow (A - 26 nmol/min, B – 34.7 nmol/min). Additional details and study of the delta doping process in β - Ga_2O_3 are reported elsewhere^{28,29}. After the delta doping process, growth of additional 21 nm β - $(Al_xGa_{1-x})_2O_3$ barrier is continued until the desired total thickness is reached (~ 23 - 25 nm including the spacer layer). The composition of the β - $(Al_xGa_{1-x})_2O_3$ barrier is controlled by setting the $[Al]/([Ga] + [Al])$ molar ratio to $x \sim 18\%$ (sample A) and $x \sim 25\%$ (sample B). In sample B, the β - $(Al_xGa_{1-x})_2O_3$ molar ratio is increased to 25% and silane flow is increased by 25% while reducing the spacer thickness to 2 nm. Composition of the β - $(Al_xGa_{1-x})_2O_3$ barrier is verified using XRD (X-ray diffraction)³⁰. The measured composition is $x=0.20$ for sample A and $x=0.27$ for sample B, which is close to the precursor molar ratio (see supplementary).

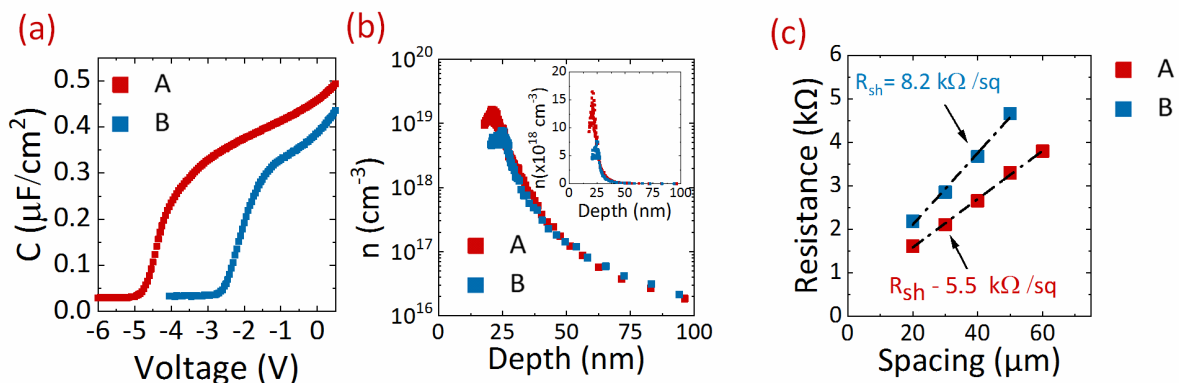


Fig.2 (a) Capacitance- Voltage measurement at room temperature (b) Extracted apparent charge density profiles for samples A and B (inset- linear scale) (c) TLM measurements of β -(Al_xGa_{1-x})₂O₃/β-Ga₂O₃ heterostructures.

FET, TLM and Van der Pauw structures were realized after mesa isolation using dry etching with SF₆/Ar chemistry (35 sccm/5 sccm, 150W RF and 600W ICP powers). Next the samples are prepared for n⁺ layer regrowth for ohmic contact formation. The samples are patterned using Ni/SiO₂ mask followed by a 50 nm etch using SF₆/Ar plasma (35 sccm/5 sccm, 150 W RF power). After the etch, Ni mask layer is removed using wet etch (diluted aqua regia) and samples are loaded in to the MOVPE reactor. Low temperature n⁺ regrowth is performed using MOVPE at a growth temperature of 600 °C. The low growth temperature is chosen to minimize any potential damage to the epitaxial layer. The doping of the n⁺ layer is set to 8 x 10¹⁹ cm⁻³ and the thickness of the n⁺ layer is 150 nm. After the completion of the n⁺ regrowth process, the SiO₂ hard mask is removed by a HF dip. Standard photolithography process is utilized for patterning Ohmic source/drain and Schottky gate pads. After the deposition of Ohmic contacts, the contacts are annealed using a RTA (Rapid thermal anneal - 90s, 450 °C) system under nitrogen environment. Both the Ohmic (30 nm Ti /100 nm Au /30 nm Ni) and Schottky contacts (30 nm Ni/50 nm Au/30 nm Ni) are deposited by ebeam evaporation.

CV, TLM and Hall measurements are utilized to independently measure apparent charge density profile, sheet charge, mobility, and sheet resistance. CV measurements performed on samples A and B are shown in fig.2(a). The apparent charge density extracted from the charge profile (including forward tail of the apparent charge profile measured until + 0.5 V) decreased from 1.1 x 10¹³ cm⁻² to 5.7 x 10¹² cm⁻² between sample A and B. Extracted apparent charge density profile of the 2DEG sheet charge is plotted in fig.2(b). Room temperature Hall measurements are also performed to measure sheet charge and mobility. Details of all the electrical measurements are summarized in Table. 1. Hall sheet charges of 1.06 x 10¹³ cm⁻² and 6.4 x 10¹² cm⁻² are recorded for sample A and B. Room temperature electron mobility values of 111 cm²/Vs and 125 cm²/Vs are measured for samples A and B, respectively. Additionally, TLM measurements are performed to extract electron channel

sheet resistance. TLM sheet resistance values of 5.5 k Ω /Square and 8.2 k Ω /Square are measured for samples A and B. The sheet charge, sheet resistance and channel mobility of Hall and TLM measurements are listed in Table 1. These electrical measurements indicate that all the measured parameters can be directly attributed to the β -(Al_xGa_{1-x})₂O₃/ β -Ga₂O₃ heterostructure channel (2DEG and parallel channel in the alloy barrier).

Table I. Hall, CV and TLM characterization of β -(Al_xGa_{1-x})₂O₃/ β -Ga₂O₃ heterostructure channel

Sample	Spacer thickness (nm)	Hall sheet charge (x 10 ¹² cm ⁻²)		Hall mobility cm ² /Vs		RT Hall Sheet resistance (k Ω /square)	RT TLM Sheet resistance (k Ω /square)
		300 K	77 K	300K	77 K		
A	4	10.6	3	111	1680	5.3	5.5
B	2	6.4	3.1	125	689	7.7	8.2

To understand the nature of the heterostructure electron channel, low temperature Hall measurements are performed at liquid nitrogen temperatures (77K). For an ideal 2DEG with no parallel channel in the β -(Al_xGa_{1-x})₂O₃ layer, the Hall measured sheet charge density is not expected to freeze out upon reaching cryogenic temperatures¹⁸). The sheet charge of samples A and B reduced to $\sim 3 \times 10^{12}$ cm⁻² at 77 K. Correspondingly, the Hall mobility increased to 1680 cm²/Vs and 689 cm²/Vs for samples A and B. The Hall measured sheet charge density reduced to 1.2 k Ω /square(sample A) and 2.9 k Ω /square(sample B) at 77K. This indicates that there is a significant amount of donor freezeout at 77 K. This reduction in sheet charge is attributed to freezeout of parallel channel in β -(Al_xGa_{1-x})₂O₃. The high low-temperature mobility observed in sample A could be potentially attributed to improved material quality of low composition β -(Al_{0.2}Ga_{0.8})₂O₃/ β -Ga₂O₃ heterointerface, compared to the higher alloy composition in sample B. Additional hall measurements through out the entire temperature range may give us more insight on carrier freeze out in β -(Al_xGa_{1-x})₂O₃ layer. In a delta-doped heterostructure with a narrow dopant profile, all the donor atoms are located in the β -(Al_xGa_{1-x})₂O₃ barrier layer. However, attaining silicon delta sheets with low

FWHM is challenging²⁸). Because of the spread-out dopant profile, non-negligible amount of charge may end up in the UID β -Ga₂O₃ layer. A finite amount of charge reduction could result from carrier freeze out in the UID β -Ga₂O₃ layer. Reports of charge freeze out at low temperature have been observed in β -(Al_xGa_{1-x})₂O₃/ β -Ga₂O₃ single and double heterostructures^{18,19,21} and uniformly doped β -(Al_xGa_{1-x})₂O₃ thin films²⁷). Based on theory, it is expected that formation of parasitic channel becomes more favorable with increasing spacer thickness. Measured Hall data also indicates similar trend. However, modeling the electron charge in this case is quite challenging due to the combination of several factors such as non-ideal delta sheet profile with spread out Si donors in the alloy barrier, incomplete ionization in the alloy barrier and unintentional doping of the UID channel due to spread of the donors. Also, the donor ionization is expected to change with different Al composition. Additionally, STEM investigations revealed formation of defects in the β -(Al_{0.28}Ga_{0.72})₂O₃ layer > 5 nm away from the heterointerface (see supplementary). The above analysis indicates that getting a very high 2DEG charge in β -(Al_xGa_{1-x})₂O₃/ β -Ga₂O₃ heterostructures is still challenging. For attaining high charge densities, it is important to realize a sharp dopant profiles in β -(Al_xGa_{1-x})₂O₃ barrier with a high conduction band offset at the β -(Al_xGa_{1-x})₂O₃/Ga₂O₃ heterojunction. Higher Al composition barrier in conjunction with thin spacer layer and sharp doping profile would be necessary to leverage the predicted high electron mobilities in β -Ga₂O₃ 2DEGs.

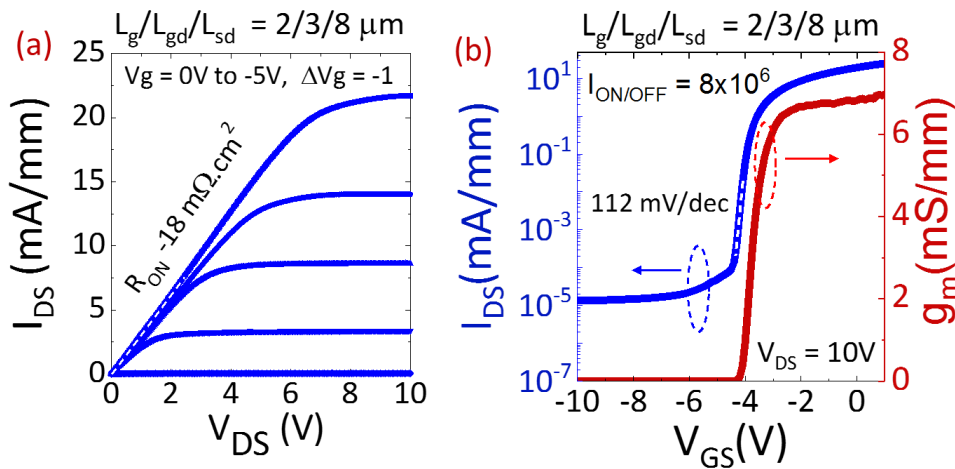


Fig.3 (a) Output and (b) transfer characteristics of β -($\text{Al}_x\text{Ga}_{1-x}$) $_2\text{O}_3$ / β - Ga_2O_3 heterostructure FET showing peak current density of 22 mA/mm ($V_{ds} = 10$ V, $V_g = 0$ V) and transconductance of 7 mS/mm ($V_{ds} = 10$ V, $V_g = 0$ V)

Lateral heterojunction field effect transistors (HFETs) are fabricated with n+ regrown contacts (sample A) with L_g , L_{sd} , L_{gd} of 2 μm , 8 μm and 3 μm respectively. Output and transfer characteristics of the FET are shown in Fig. 3(a) and 3(b). The devices showed a peak current of 22 mA/mm at zero gate bias and drain bias of 10 V. From the TLM measurements, the contact resistance to the heterostructure channel was extracted to be as high as 16.5 ohm.mm. MOVPE films grown at low temperature showed high mobility and low compensation²⁴). TLM measurements on regrown n+ layer without any channel layer, showed a $\rho_c \sim 10^{-6} \Omega\text{-cm}^2$ indicating low resistance n+ Ga_2O_3 /Ti contact. The high R_c is attributed to etch damage and charge depletion due to Fluorine ions³¹) resulting from the SF_6 /Ar dry etch step used before the contact regrowth step. Switching to BCl_3 /Ar chemistry-based dry etch step could lead to lower contact resistivity. The peak current is currently limited by the device dimension and the performance of the source/drain ohmic contacts. The device showed good pinch off characteristics with a pinch off voltage close of -4 V, correlating well with the CV measurements. The device also showed a high on-off ratio of 8×10^6 and sub-threshold swing of 112 mV/dec. A peak transconductance of 7 mS/mm is measured at zero gate bias.

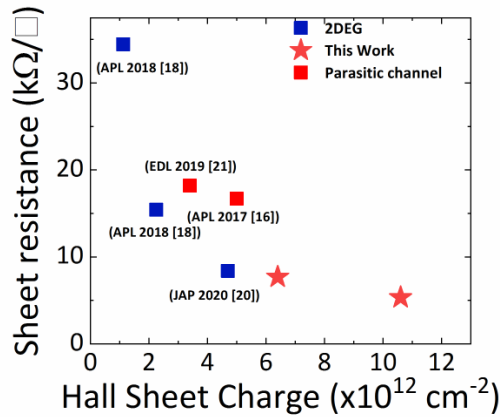


Fig. 4 Comparison of measured Hall sheet resistance as a function of charge density for a single $\beta\text{-(Al}_x\text{Ga}_{1-x})_2\text{O}_3/\beta\text{-Ga}_2\text{O}_3$ heterostructure channel.

The measured room temperature sheet resistance values are plotted as a function of the charge density in fig.4 (see supplementary for Hall measurement data). In this work, we report a low sheet resistance value of 5.3 k Ω /Square for a single $\beta\text{-(Al}_x\text{Ga}_{1-x})_2\text{O}_3/\beta\text{-Ga}_2\text{O}_3$ heterostructure. Additionally, we report $\beta\text{-(Al}_x\text{Ga}_{1-x})_2\text{O}_3/\beta\text{-Ga}_2\text{O}_3$ heterostructure device grown and fabricated completely based on MOVPE process, including contact regrowth. However, the complete charge cannot be ascribed to modulation-doped carriers because of parallel channel in $\beta\text{-(Al}_x\text{Ga}_{1-x})_2\text{O}_3$ layer as evidenced from observed carrier freezeout at low temperature. Nevertheless, the low sheet resistance value obtained in this work, with room temperature mobilities exceeding 100 cm²/Vs is a promising step towards high performance MOVPE-grown $\beta\text{-(Al}_x\text{Ga}_{1-x})_2\text{O}_3/\beta\text{-Ga}_2\text{O}_3$ modulation-doped devices.

In conclusion, we report on growth and characterization of MOVPE-grown $\beta\text{-(Al}_x\text{Ga}_{1-x})_2\text{O}_3/\beta\text{-Ga}_2\text{O}_3$ heterostructure channel with low sheet resistance. Electrical characteristics of the heterostructure channel are measured using TLM, CV and Hall measurements. Room temperature Hall measurements showed a high sheet charge of $6.4 \times 10^{12} - 1.06 \times 10^{13}$ cm⁻² and mobility of 111-125 cm²/Vs. STEM investigation of $\beta\text{-(Al}_x\text{Ga}_{1-x})_2\text{O}_3/\beta\text{-Ga}_2\text{O}_3$ heterostructure showed formation of defects away from the interface. FET showed a peak current density of 22 mA/mm and on-off ratio of 8×10^6 .

Acknowledgments

This material is based upon work supported by the Air Force Office of Scientific Research under award number FA9550-18-1-0507 and monitored by Dr. Ali Sayir. Any opinions, findings, conclusions, or recommendations expressed in this material are those of the authors and do not necessarily reflect the views of the United States Air Force. Praneeth Ranga acknowledges support from University of Utah Graduate Research Fellowship 2020-2021. This work was performed in part at the Utah Nanofab sponsored by the College of Engineering and the Office of the Vice President for Research. The authors thank the Air Force Research Laboratory's Sensors Directorate for their discussions with them. The electron microscopy work was performed in the Materials Characterization lab (MCL) at the Materials Research Institute (MRI) at the Pennsylvania State University. The work at PSU was supported by the AFOSR program FA9550-18-1-0277 (GAME MURI, Dr. Ali Sayir, Program Manager).

References

- 1) M. Higashiwaki, K. Sasaki, A. Kuramata, T. Masui, and S. Yamakoshi, *Appl. Phys. Lett.* **100**, 013504 (2012).
- 2) K. Goto, K. Konishi, H. Murakami, Y. Kumagai, B. Monemar, M. Higashiwaki, A. Kuramata, and S. Yamakoshi, *Thin Solid Films* **666**, 182 (2018).
- 3) Z. Feng, A.F.M.A.U. Bhuiyan, Z. Xia, W. Moore, Z. Chen, J.F. McGlone, D.R. Daughton, A.R. Arehart, S.A. Ringel, S. Rajan, and H. Zhao, *Phys. Status Solidi RRL – Rapid Res. Lett.* **14**, 2000145 (2020).
- 4) S. Rafique, M.R. Karim, J.M. Johnson, J. Hwang, and H. Zhao, *Appl. Phys. Lett.* **112**, 052104 (2018).
- 5) K. Sasaki, A. Kuramata, T. Masui, E.G. Villora, K. Shimamura, and S. Yamakoshi, *Appl. Phys. Express* **5**, 035502 (2012).
- 6) S.J. Pearton, F. Ren, M. Tadjer, and J. Kim, *J. Appl. Phys.* **124**, 220901 (2018).
- 7) Z. Xia, H. Xue, C. Joishi, J. Mcglone, N.K. Kalarickal, S.H. Sohel, M. Brenner, A. Arehart, S. Ringel, S. Lodha, W. Lu, and S. Rajan, *IEEE Electron Device Lett.* **40**, 1052 (2019).
- 8) A.J. Green, K.D. Chabak, E.R. Heller, R.C. Fitch, M. Baldini, A. Fiedler, K. Irmscher, G. Wagner, Z. Galazka, S.E. Tetlak, A. Crespo, K. Leedy, and G.H. Jessen, *IEEE Electron Device Lett.* **37**, 902 (2016).
- 9) W. Li, K.Nomoto, Z.Hu, T.Nakamura, D.Jena and H.G. Xing in 2019 IEEE International Electron Devices Meeting (IEDM) (pp. 12-4)
- 10) N.K. Kalarickal, Z. Feng, A.F.M. Bhuiyan, Z. Xia, J.F. McGlone, W. Moore, A.R. Arehart, S.A. Ringel, H. Zhao, and S. Rajan, *ArXiv Prepr. ArXiv200602349* (2020).
- 11) S. Sharma, K. Zeng, S. Saha, and U. Singiseti, *IEEE Electron Device Lett.* **41**, 836 (2020).
- 12) N. Ma, N. Tanen, A. Verma, Z. Guo, T. Luo, H. (Grace) Xing, and D. Jena, *Appl. Phys. Lett.* **109**, 212101 (2016).
- 13) H. Peelaers, J.B. Varley, J.S. Speck, and C.G. Van de Walle, *Appl. Phys. Lett.* **112**, 242101 (2018).

- 14) J.B. Varley, A. Perron, V. Lordi, D. Wickramaratne, and J.L. Lyons, *Appl. Phys. Lett.* **116**, 172104 (2020).
- 15) A. Kumar, K. Ghosh, and U. Singiseti, *J. Appl. Phys.* **128**, 105703 (2020).
- 16) S. Krishnamoorthy, Z. Xia, C. Joishi, Y. Zhang, J. McGlone, J. Johnson, M. Brenner, A.R. Arehart, J. Hwang, and S. Lodha, *Appl. Phys. Lett.* **111**, 023502 (2017).
- 17) E. Ahmadi, O.S. Koksaldi, X. Zheng, T. Mates, Y. Oshima, U.K. Mishra, and J.S. Speck, *Appl. Phys. Express* **10**, 071101 (2017).
- 18) Y. Zhang, A. Neal, Z. Xia, C. Joishi, J.M. Johnson, Y. Zheng, S. Bajaj, M. Brenner, D. Dorsey, K. Chabak, G. Jessen, J. Hwang, S. Mou, J.P. Heremans, and S. Rajan, *Appl. Phys. Lett.* **112**, 173502 (2018).
- 19) Y. Zhang, C. Joishi, Z. Xia, M. Brenner, S. Lodha, and S. Rajan, *Appl. Phys. Lett.* **112**, 233503 (2018).
- 20) N.K. Kalarickal, Z. Xia, J.F. McGlone, Y. Liu, W. Moore, A.R. Arehart, S.A. Ringel, and S. Rajan, *J. Appl. Phys.* **127**, 215706 (2020).
- 21) C. Joishi, Y. Zhang, Z. Xia, W. Sun, A.R. Arehart, S. Ringel, S. Lodha, and S. Rajan, *IEEE Electron Device Lett.* 40(8), pp.1241-1244. (2019).
- 22) Z. Feng, A.F.M. Anhar Uddin Bhuiyan, M.R. Karim, and H. Zhao, *Appl. Phys. Lett.* **114**, 250601 (2019).
- 23) S. Bin Anooz, R. Grüeneberg, T.-S. Chou, A. Fiedler, K. Irmscher, C. Wouters, R. Schewski, M. Albrecht, Z. Galazka, W. Miller, J. Schwarzkopf, and A. Popp, *J. Phys. Appl. Phys.* 54, 034003 (2020).
- 24) A. Bhattacharyya, P. Ranga, S. Roy, J. Ogle, L. Whittaker-Brooks, and S. Krishnamoorthy, *Appl. Phys. Lett.* **117**, 142102 (2020).
- 25) A.F.M.A.U. Bhuiyan, Z. Feng, J.M. Johnson, H.L. Huang, J. Hwang, and H. Zhao, *Cryst. Growth Des.* 20(10), 6722-6730 (2020).
- 26) A.F.M. Anhar Uddin Bhuiyan, Z. Feng, J.M. Johnson, Z. Chen, H.-L. Huang, J. Hwang, and H. Zhao, *Appl. Phys. Lett.* **115**, 120602 (2019).
- 27) P. Ranga, A. Rishinaramangalam, J. Varley, A. Bhattacharyya, D. Feezell, and S. Krishnamoorthy, *Appl. Phys. Express* **12**, 111004 (2019).
- 28) P. Ranga, A. Bhattacharyya, A. Rishinaramangalam, Y.K. Ooi, M.A. Scarpulla, D. Feezell, and S. Krishnamoorthy, *Appl. Phys. Express* **13**, 045501 (2020).
- 29) P. Ranga, A. Bhattacharyya, A. Chmielewski, S. Roy, N. Alem, and S. Krishnamoorthy, *Appl. Phys. Lett.* **117**, 172105 (2020).

30) Y. Oshima, E. Ahmadi, S.C. Badescu, F. Wu, and J.S. Speck, *Appl. Phys. Express* **9**, 061102 (2016).

31) J. Yang, C. Fares, F. Ren, R. Sharma, E. Patrick, M.E. Law, S.J. Pearton, and A. Kuramata, *J. Appl. Phys.* **123**, 165706 (2018).

Figure Captions

Fig. 1. Schematic of MOVPE-grown β -(Al_xGa_{1-x})₂O₃/ β -Ga₂O₃ heterostructure FET (HFET) with regrown ohmic contacts. (Sample A spacer layer thickness- 4 nm; Sample B spacer layer thickness- 2 nm).

Fig. 2. (a) Capacitance- Voltage measurements at room temperature (b) Extracted apparent charge density profiles for samples A and B (inset-linear scale)(c) TLM measurements of β -(Al_xGa_{1-x})₂O₃/ β -Ga₂O₃ heterostructures.

Fig. 3. (a) Output and (b) transfer characteristics of β -(Al_xGa_{1-x})₂O₃/ β -Ga₂O₃ heterostructure FET showing peak current density of 22 mA/mm ($V_{ds} = 10$ V, $V_g = 0$ V) and transconductance of 7 mS/mm ($V_{ds} = 10$ V, $V_g = 0$ V)

Fig. 4. Comparison of measured Hall sheet resistance as a function of charge density for a single β -(Al_xGa_{1-x})₂O₃/ β -Ga₂O₃ heterostructure channel.

Figure 1

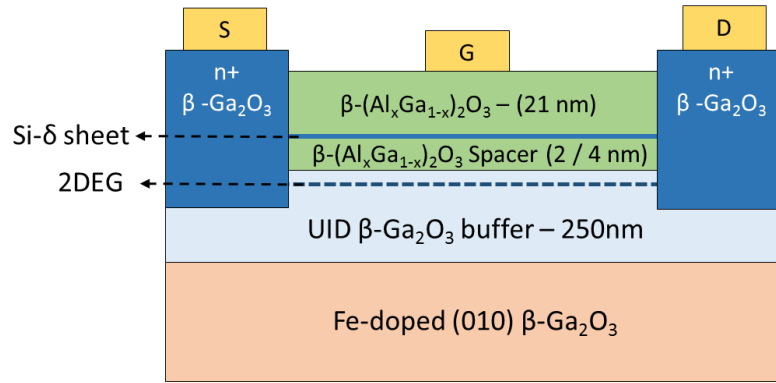


Figure 2

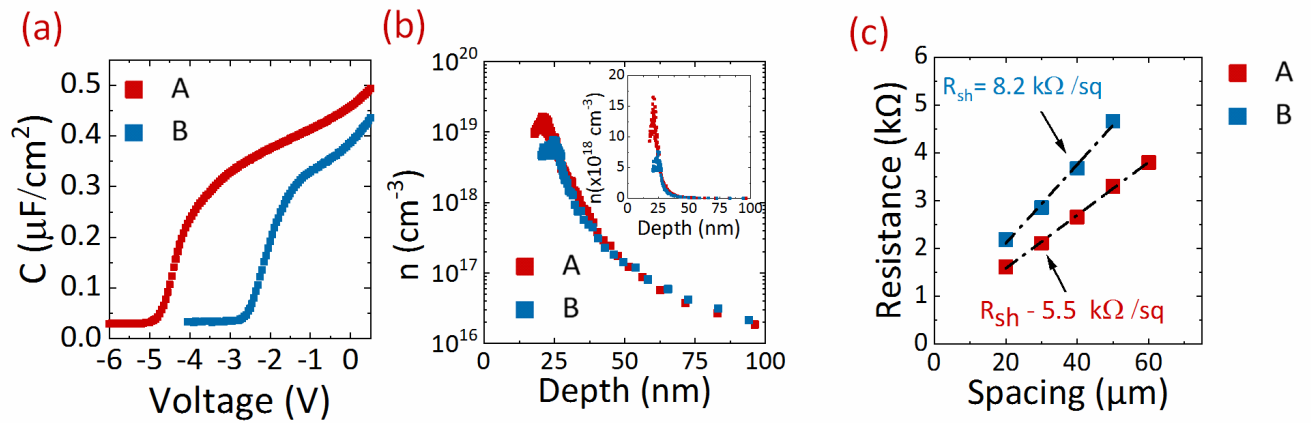


Figure 3

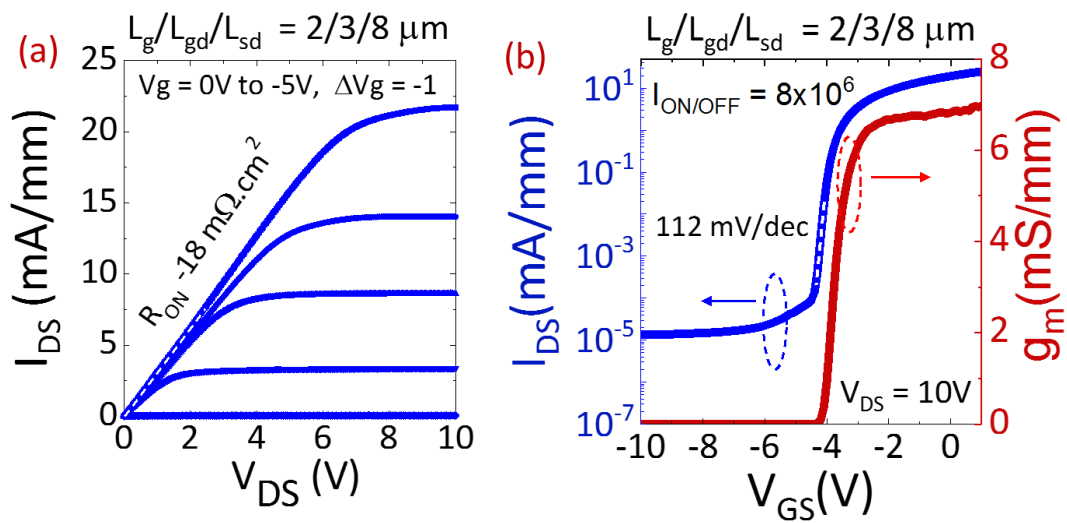
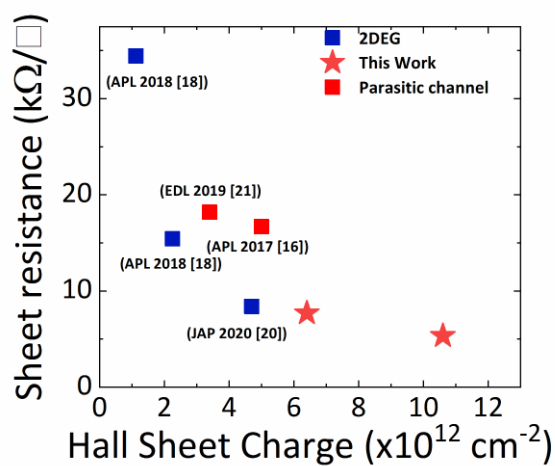


Figure 4



Growth and Characterization of Metalorganic Vapor-Phase Epitaxy-Grown β -(Al_xGa_{1-x})₂O₃/β-Ga₂O₃ Heterostructure Channels

Praneeth Ranga^{1, a)}, Arkka Bhattacharyya^{1, a)}, Adrian Chmielewski², Saurav Roy¹, Rujun Sun¹, Michael A. Scarpulla^{1,3}, Nasim Alem² and Sriram Krishnamoorthy¹

¹ Department of Electrical and Computer Engineering, The University of Utah, Salt Lake City, UT 84112, United States of America

² Department of Materials Science and Engineering, Pennsylvania State University, University Park, State College, PA 16802, USA

³ Department of Materials Science and Engineering, University of Utah, Salt Lake City, Utah 84112, USA

a) Praneeth Ranga and Arkka Bhattacharyya contributed equally to this work.

Supplementary information

X ray diffraction scan of β -(Al_xGa_{1-x})₂O₃/Ga₂O₃ heterostructures

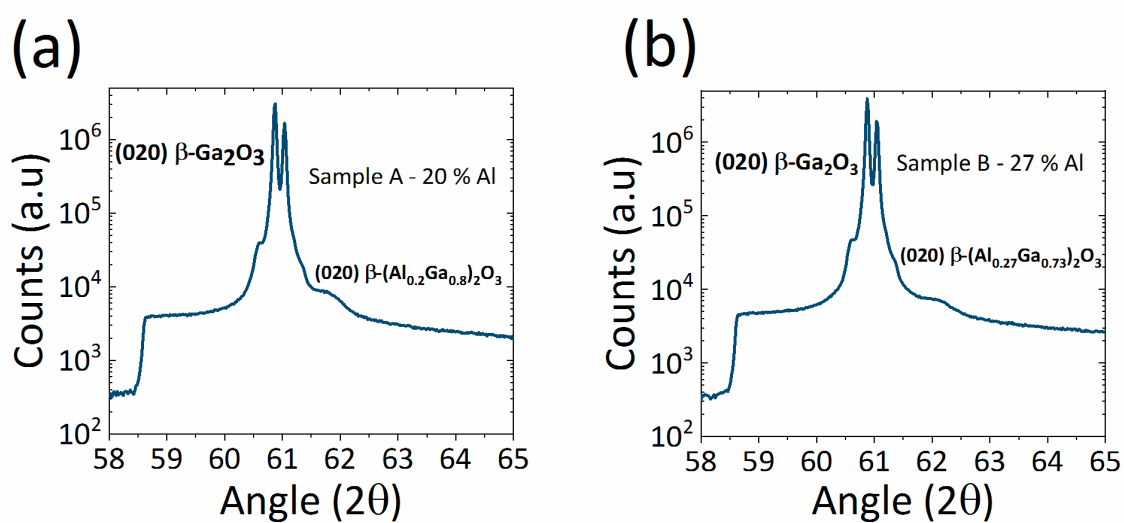


Fig.S1 XRD scan of β -(Al_xGa_{1-x})₂O₃/β-Ga₂O₃ heterostructure (a) Sample A (20% - Al) (b) Sample B (27% - Al). Incident X-ray has both Kα₁ and K α₂ wavelengths.

STEM images of β -(Al_{0.28}Ga_{0.72})₂O₃/ β -Ga₂O₃ interface

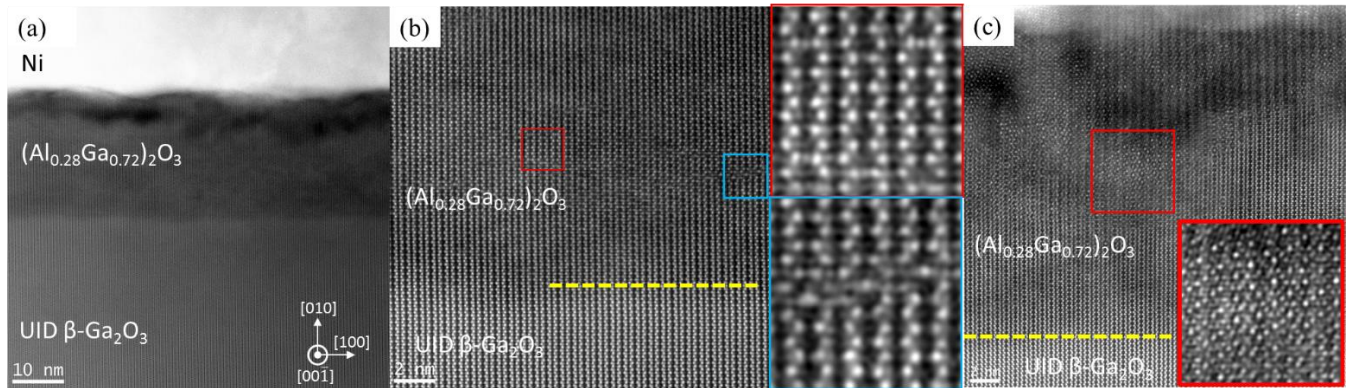


Fig. S2 (a) HAADF-STEM image of the β -(Al_{0.28}Ga_{0.72})₂O₃/ β -Ga₂O₃ interface in the [00 $\bar{1}$] projection at low magnification (b) zoomed-in image of the β -(Al_{0.28}Ga_{0.72})₂O₃/ β -Ga₂O₃ heterostructure showing defect formation in β -(Al_{0.28}Ga_{0.72})₂O₃ layer (inset: high magnification image of the defect region) (c) HAADF-STEM image of β -(Al_{0.28}Ga_{0.72})₂O₃/ β -Ga₂O₃ heterostructure showing defect formation (inset: high magnification image of the defective region)

High resolution high angle annular dark field-scanning transmission electron microscopy (HAADF-STEM) investigations are performed on β -(Al_{0.28}Ga_{0.72})₂O₃/ β -Ga₂O₃ grown on Sn-doped (010) β -Ga₂O₃ structures with growth conditions identical to sample B (2 nm spacer). HAADF-STEM imaging is carried out using a FEI Titan G2 60-300 transmission electron microscope (TEM) at 300kV. A condenser aperture of 70 μ m is used with a convergence angle of 30 mrad and the annular detector collection angles in the 42-250 mrad range. The camera length is set to 1.15m and the probe current is approximately 80 pA. As the contrast is proportional to the Z number of the atom in the STEM mode, the heavier the atom, the brighter it will appear on the projected image. Figure S2(a) is a HAADF-STEM image of the β -(Al_{0.28}Ga_{0.72})₂O₃/ β -Ga₂O₃ interface in the [00 $\bar{1}$] projection at low magnification. This zone axis allows to have the distance between Ga atoms easily resolved

by the TEM. The top of the image corresponds to the Nickel contact layer whereas the β - $(\text{Al}_{0.28}\text{Ga}_{0.72})_2\text{O}_3/\beta\text{-Ga}_2\text{O}_3$ interface is easily observable due to the contrast change. A zoom-in image of the interface is shown in fig. S2(b). The yellow dashed lines represents the heterostructure interface. The $\beta\text{-Ga}_2\text{O}_3$ substrate has a homogeneous bright contrast whereas the $\beta\text{-}(\text{Al}_{0.28}\text{Ga}_{0.72})_2\text{O}_3$ film is darker overall which is due to the presence of lighter Al atoms. Interestingly, different types of point defects are observed in the $\beta\text{-}(\text{Al}_{0.28}\text{Ga}_{0.72})_2\text{O}_3$ film such as Al/Ga interstitials and Ga vacancies. Some of these defects have already been studied in the literature. For instance, Johnson et al. have shown the formation of Ga interstitial sitting in between two Ga vacancies creating a 2VGa-Ga_i complex in Sn doped $\beta\text{-Ga}_2\text{O}_3$ ¹⁾. More recently, A. Chmielewski et al. reported the formation of di-interstitial di-vacancy complexes at the MBE grown $\beta\text{-}(\text{Al}_{0.2}\text{Ga}_{0.8})_2\text{O}_3/\beta\text{-Ga}_2\text{O}_3$ interface that are created by either an Al or Ga interstitial in the tetrahedral site²⁾.

Figure. S2(c) is a HAADF-STEM image of another area of the sample. A zoom-in image of the defective area is shown in the red square in which a similar structure to the γ -phase is observed. A mixture of β and γ phases in MOCVD grown $\beta\text{-}(\text{Al}_x\text{Ga}_{1-x})_2\text{O}_3$, when Al composition ranged between 27% and 40%, has already been reported in the literature³⁾. Although these contrast are very similar to those of a γ -phase, similar structures were observed when two β -lattices with a relative shift of 2.72 \AA in the $\langle 102 \rangle$ direction are superimposed along the $\langle 010 \rangle$ viewing direction⁴⁾. As of now, there is no general consensus towards the understanding of this contrast and a deeper analysis will be necessary to have a better comprehension of it. However, here, it is clearly observable that these defects are present further from the $\beta\text{-}(\text{Al}_{0.28}\text{Ga}_{0.72})_2\text{O}_3/\beta\text{-Ga}_2\text{O}_3$ interface as shown by the inserts in Figure S2(b).

Low temperature capacitance-voltage extracted apparent charge density

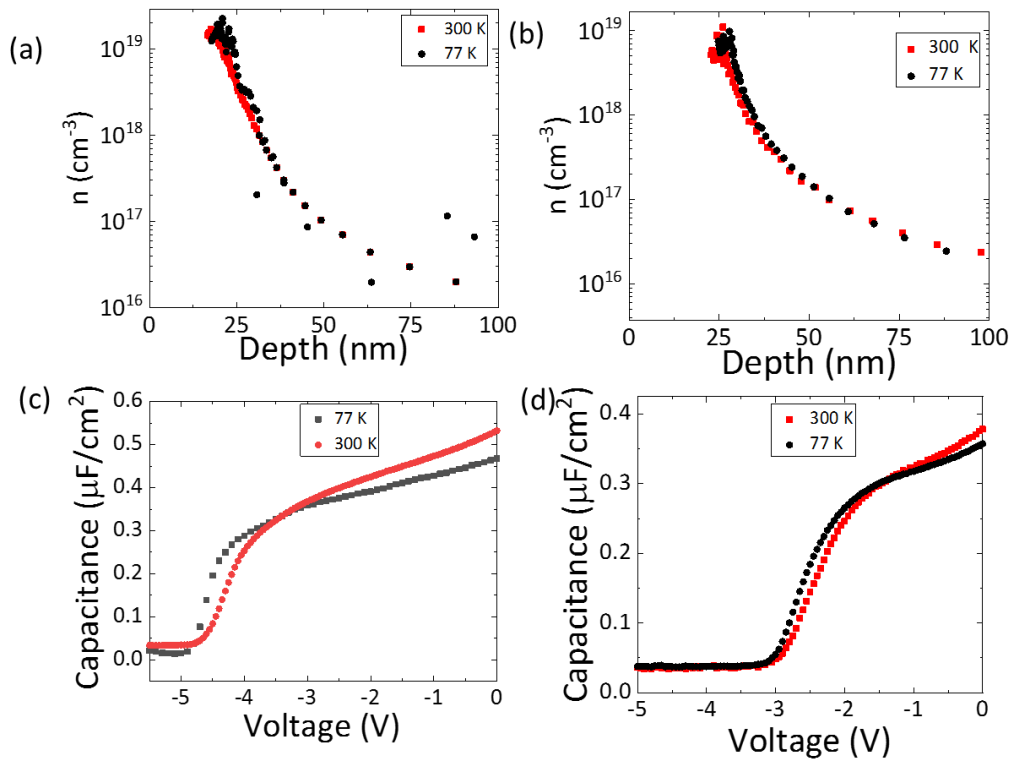


Fig.S3 Capacitance-voltage data of a) sample A and b) Sample B measured at 300 K and 77 K. Apparent charge density profile extracted from capacitance-voltage measurements at 77 K and 300 K (c) Sample A (d) Sample B

CV measurements of the β -(Al_xGa_{1-x})₂O₃/β-Ga₂O₃ heterostructure revealed no significant difference upon going from 300 K to 77 K. However, low temperature hall measurements clearly showed carrier freeze out. This discrepancy can be explained by understanding that CV extracted charge density doesn't follow the actual carrier profile at 77 K. Instead, CV measures the apparent charge profile (donor density), leading to observation of high apparent

charge density at 77 K, whereas, Hall measurement can only measure free carriers present in the β -(Al_xGa_{1-x})₂O₃/β-Ga₂O₃ channel layer. It should be noted that the amount of ionization of the donors also change with reverse bias, further complicating the interpretation of CV measurements.

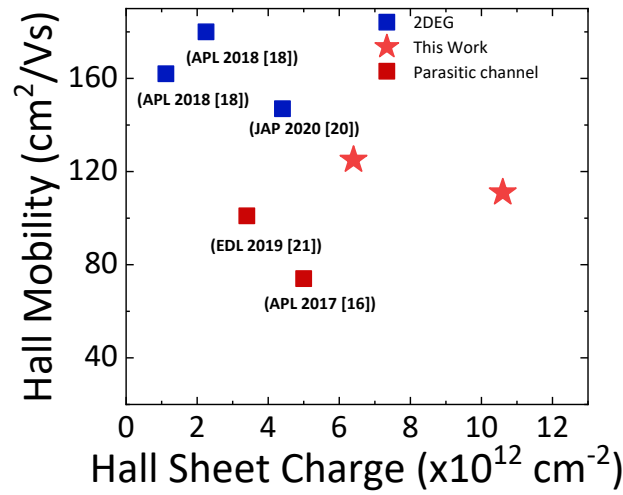


Fig. S4 Hall mobility plotted against Hall sheet charge for β -(Al_xGa_{1-x})₂O₃/β-Ga₂O₃ heterostructure in literature

References

- J.M. Johnson, Z. Chen, J.B. Varley, C.M. Jackson, E. Farzana, Z. Zhang, A.R. Arehart, H.-L. Huang, A. Genc, S.A. Ringel, C.G. Van de Walle, D.A. Muller, and J. Hwang, *Physical Review X* **9**, (2019).
- A. Chmielewski, S. Deng, P. Moradifar, L. Miao, K.A. Lopez, A. Mauze, Y. Zhang, J. Speck, W. Windl, and N. Alem, *Microscopy and Microanalysis* **25**.S2 (2019): 2186-2187
- A.F.M.A.U. Bhuiyan, Z. Feng, J.M. Johnson, H.-L. Huang, J. Sarker, M. Zhu, M.R. Karim, B. Mazumder, J. Hwang, and H. Zhao, *APL Materials* **8**, 031104 (2020).
- C. Wouters, R. Schewski, and M. Albrecht, *APL Materials* **8**, 089101 (2020).

Template for APEX (Jan. 2014)